Superelastic scattering with imperfect laser polarization

R. E. Scholten
School of Physics, University Of Melbourne, Parkville, Victoria 3052, Australia

V. Karaganov and P. J. O. Teubner
Physics Department, Flinders University of South Australia, G.P.O. Box 2100, Adelaide 5001, Australia

P. M. Farrell
Optical Technology Research Laboratory, Victoria University, Footscray 8001, Australia
(Received 15 January 1999)

The formalism applied to superelastic electron scattering from laser-excited atoms has to date assumed perfect polarization of the laser light. We consider the effects of imperfect polarization, deriving an expression for the superelastic scattering rate from target atoms optically pumped with elliptically polarized light, and show how imperfect polarization effects can be measured and minimized under experimental conditions. In particular, we find that in measuring the scattering for linearly polarized light with a small circular component, the errors are proportional to the undesired circular polarization component and to $\bar{P}_3$, the scattering sensitivity to circular light. We also present in detail a polarizer design which generates both linear and circular polarizations, allowing measurement of all scattering polarization sensitivities without requiring interchange of optical elements. [S1050-2947(99)03007-3]

PACS number(s): 34.80.Dp, 42.79.Ci

I. INTRODUCTION

Superelastic scattering from laser-excited atoms provides a powerful technique for testing theoretical models of inelastic electron-atom collision processes [1]. In these experiments, the target atoms are prepared in a well-defined quantum state by optical pumping; that is, by repeated excitation and spontaneous decay, using polarized laser light. Electrons are scattered from the laser-prepared atoms, and detected at some scattering angle θ_e. Using an energy-selective filter, only superelastic electrons (those which gain energy through collision with atoms in the excited state) are counted. The scattering rate is measured as a function of the laser polarization and hence the quantum state of the target atoms.

A detailed knowledge of the laser-prepared target state is required to extract the atomic collision parameters from the measured scattering rates. This can be calculated, or to some extent measured, but in either case the formalism has generally assumed perfect polarization of the laser light, which excludes coherent excitation of multiple magnetic substates. Unfortunately, the polarization can be imperfect: elliptical rather than perfectly linear or circular, or with the polarization axis misaligned with respect to the scattering geometry.

We investigate the effects of imperfectly polarized light on the measured scattering parameters, first by extending the theoretical formalism to include elliptically polarized light with arbitrary alignment angle (Sec. III). The polarization errors are related to the design and implementation of the apparatus used to polarize the laser beam. Section IV evaluates potential causes, in particular, for a type of polarizer which has significant advantages for these experiments. The polarization errors lead to effects in the scattering parameters which can easily be measured and minimized during the course of a typical superelastic scattering experiment; these processes are described in Sec. VI. Finally, the systematic errors due to imperfect polarization can be conveniently estimated for all scattering angles using measurements at just one angle (Sec. VII).

These results offer practical and powerful methods for analyzing the effects of polarization components and solving polarization-related problems in superelastic experiments.

II. SUPERELASTIC SCATTERING WITH ELLIPTICAL POLARIZATION

Our discussion is relevant to a broad range of laser-excited superelastic experiments, but for clarity we specifically consider the popular *s-p* transitions, and, in particular, an example taken from our recent work on low-energy electron scattering from lithium [2]. Figure 1 shows the experimental arrangement, which has been described in some detail earlier [2]. Li^6 atoms are first laser excited to the $2\,^2P_{3/2}$ manifold with laser light at 670.977 nm (*in vacuo*). Because of the small hyperfine splittings, all the excited hyperfine levels are coherently excited. Two-frequency pumping is used to prevent trapping in the $\bar{F}=1/2$ ground state.

Electrons of energy E_0 collisionally deexcite the atoms to the $2\,^2S_{1/2}$ ground states and gain 1.8 eV in energy. The superelastic electrons are detected at scattering angle θ_e, and the rate measured as a function of the laser polarization. The reaction is

$$\mathrm{Li}(2\,^2P_{3/2})+e(\boldsymbol{k}_{\mathrm{in}},E_0-1.8\ \mathrm{eV})\rightarrow\mathrm{Li}(2\,^2S_{1/2})+e(\boldsymbol{k}_{\mathrm{out}},E_0),$$

where E_0 is the scattered superelastic electron energy and $\boldsymbol{k}_{\mathrm{in,out}}$ are the momentum vectors for the incident and scattered electrons.

The electron scattering rate for a given scattering angle, normalized to the differential cross section, is given by

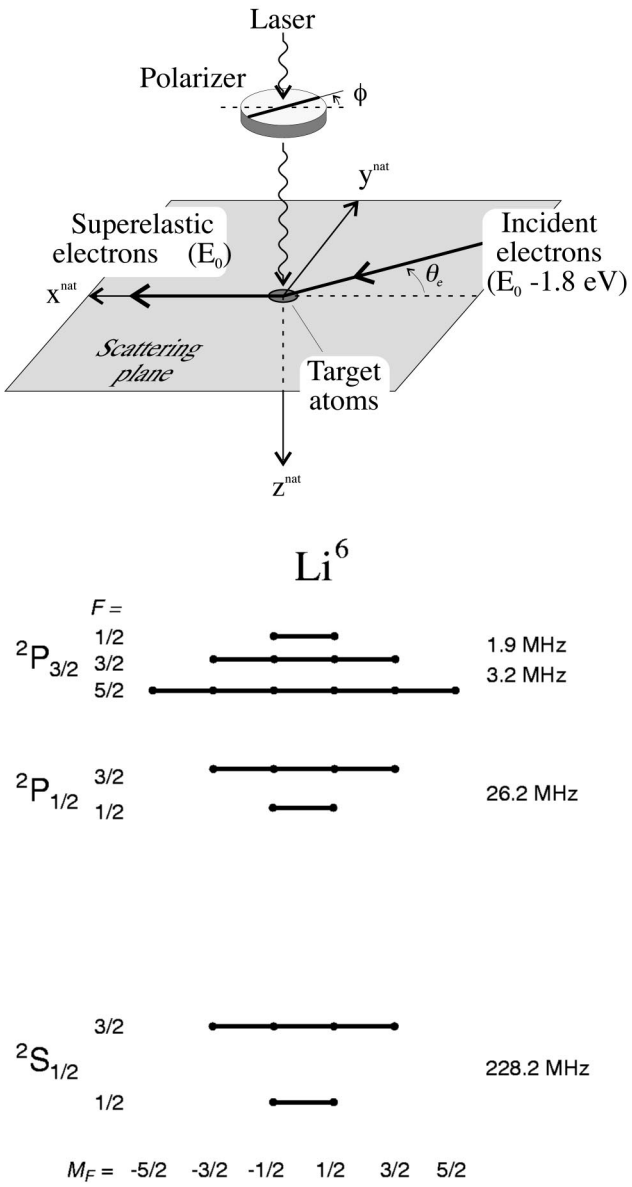

FIG. 1. Superelastic scattering geometry in the natural frame of Andersen *et al.* [1], and Li^6 energy levels (not to scale). The $2\,^2S_{1/2}\rightarrow 2\,^2P_{3/2}$ transition has a wavelength of 670.977 nm (*in vacuo*). The hyperfine splitting frequencies are also shown on the right.

$$\mathcal{I}=\mathrm{tr}(\rho\sigma), \tag{1}$$

where the collisional density matrix ρ depends solely on the scattering amplitudes, and σ is the density matrix describing the laser-excited target atoms, which depends on the laser polarization and optical pumping processes. ρ is normalized but the trace of σ depends on the excitation fraction which can vary with laser parameters such as intensity, frequency, linewidth, and polarization. The collisional density matrix can be extracted by measuring the scattering rates for different σ, which are obtained by changing the laser polarization.

The formalism which relates measurable scattering rates for different (perfect) laser polarizations to the desired elements of the collisional density matrix is given in [4]. We follow the same derivation, but allow for the additional off-diagonal terms introduced by imperfect laser polarizations.

The optical pumping process evolves slowly and hence involves the fully hyperfine-coupled FM_F angular momentum structure of the target. For excitation with laser light in a pure polarization state, a single quantization axis can be chosen such that there are no coherent excitations of multiple magnetic substates. The trace of Eq. (1) is therefore simply a sum over the appropriate matrix elements, diagonal in M_F, as given in Eq. (5) of [4]:

$$\mathcal{I}=\sum_{FM_F\bar{F}} \rho^L_{FM_F\bar{F}M_F}\sigma^L_{FM_F\bar{F}M_F}, \tag{2}$$

where the overbar indicates ground states and the superscript L indicates the quantization reference frame for the laser polarization. The quantization axis is most conveniently the direction of electric field oscillation for linearly polarized light, and along the laser propagation axis for circular light.

Elliptically polarized pumping leads to the coherent population of multiple excited magnetic substates (see [5]), and so the scattering rate becomes

$$\mathcal{I}=\sum_{FM_F\bar{F}\bar{M}_F} \rho^L_{FM_F\bar{F}\bar{M}_F}\sigma^L_{FM_F\bar{F}\bar{M}_F}. \tag{3}$$

We reduce the scattering matrix ρ^L to the LM_L basis using the standard reduction formulas, as in Eqs. (6) and (7) of [4], and the scattering intensity can then be written as

$$\mathcal{I}=a\rho^L_{11}+b\rho^L_{00}+c\rho^L_{10}+d\rho^L_{1-1}+e\rho^L_{0-1}, \tag{4}$$

where a,b are real and c–e are complex. $\rho^L_{M_L\bar{M}_L}$ are the reduced scattering matrix elements in the laser reference frame, and the coefficients a–e depend on the target density matrix elements, $\sigma^L_{FM_F\bar{F}\bar{M}_F}$. The relationships between a–e and $\sigma^L_{FM_F\bar{F}\bar{M}_F}$ are similar to those in Eq. (9) of [4] but the increased complexity due to the additional off-diagonal terms precludes their inclusion here.

The scattering matrix is most appropriately described in the *natural* reference frame which is defined by the collision geometry (Fig. 1), rather than in the laser reference frame used for the target matrix. Hence we rotate ρ^L from the laser frame to the natural frame. In the laser frame, the quantization axis is along the major axis of the polarization ellipse (for nominally linear polarizations) and along the laser beam for nominally circular light. The natural frame has quantization axis perpendicular to the scattering plane (i.e., along the direction of laser propagation). We rotate the reference from the laser frame to the natural frame, therefore finding the laser-frame density matrix in terms of the natural-frame matrix elements. The Euler angles [12] (for nominally linearly polarized light) are $(\alpha,\beta,\gamma)=(\pi/2,-\pi/2,\phi)$, where ϕ is the polarization angle (Fig. 1), and so

$$\rho^L_{11}=\frac{1}{4}+\frac{1}{2}(\cos 2\phi\,\mathrm{Re}\,\rho^{\mathrm{nat}}_{1-1}+\sin 2\phi\,\mathrm{Im}\,\rho^{\mathrm{nat}}_{1-1}), \tag{5a}$$

$$\rho_{10}^{L}=\frac{i}{2\sqrt{2}}(2\rho_{11}^{\mathrm{nat}}-1)+\frac{1}{\sqrt{2}}(\cos 2\phi\,\mathrm{Im}\,\rho_{1-1}^{\mathrm{nat}} - \sin 2\phi\,\mathrm{Re}\,\rho_{1-1}^{\mathrm{nat}}), \tag{5b}$$

$$\rho_{1-1}^{L}=-\frac{1}{4}-\frac{1}{2}(\cos 2\phi\,\mathrm{Re}\,\rho_{1-1}^{\mathrm{nat}}+\sin 2\phi\,\mathrm{Im}\,\rho_{1-1}^{\mathrm{nat}}), \tag{5c}$$

$$\rho_{00}^{L}=\frac{1}{2}-(\cos 2\phi\,\mathrm{Re}\,\rho_{1-1}^{\mathrm{nat}}+\sin 2\phi\,\mathrm{Im}\,\rho_{1-1}^{\mathrm{nat}}), \tag{5d}$$

$$\rho_{0-1}^{L}=\frac{i}{2\sqrt{2}}(2\rho_{11}^{\mathrm{nat}}-1)-\frac{1}{\sqrt{2}}(\cos 2\phi\,\mathrm{Im}\,\rho_{1-1}^{\mathrm{nat}} - \sin 2\phi\,\mathrm{Re}\,\rho_{1-1}^{\mathrm{nat}}). \tag{5e}$$

The superelastic collision rate for targets prepared by optical pumping with elliptically polarized light can then be written in terms of the scattering density matrix in the natural scattering frame, by simply substituting these expressions for ρ^{L} into Eq. (4).

III. SCATTERING RATE POLARIZATION SENSITIVITY

Information on the scattering process, described by ρ^{nat}, is extracted by measuring the scattering rate as a function of the laser polarization. ρ^{nat} has only three independent real parameters [1], which are generally determined by measuring polarization sensitivities P_i. Using linearly polarized light incident normal to the scattering plane, we measure

$$P_1=\frac{\mathcal{I}_0-\mathcal{I}_{90}}{\mathcal{I}_0+\mathcal{I}_{90}}, \qquad P_2=\frac{\mathcal{I}_{45}-\mathcal{I}_{135}}{\mathcal{I}_{45}+\mathcal{I}_{135}}, \tag{6}$$

where $\mathcal{I}_{\phi}$ is the superelastic count rate when the laser light is polarized at angle ϕ with respect to the scattered electron trajectory. By using circularly polarized light, we find

$$P_3=\frac{\mathcal{I}_{\mathrm{RHC}}-\mathcal{I}_{\mathrm{LHC}}}{\mathcal{I}_{\mathrm{RHC}}+\mathcal{I}_{\mathrm{LHC}}}, \tag{7}$$

where $\mathcal{I}_{\mathrm{RHC,LHC}}$ are count rates for right and left hand circular polarizations, respectively.

The measured polarization sensitivities P_i depend on both the scattering process and the target preparation. The target state dependence is normally removed by defining *reduced* parameters $\overline{P}_i$, which represent scattering for the ideal P state in an LM_L basis [1]. The reduced parameters are directly related to the scattering density matrix elements in the LM_L basis [1],

$$\rho^{\mathrm{nat}}=\langle\overline{M}_L|\rho|M_L\rangle=\frac{1}{2}\begin{pmatrix}1+L_{\perp} & 0 & -\overline{P}_l e^{-2i\gamma}\\ 0 & 0 & 0\\ -\overline{P}_l e^{+2i\gamma} & 0 & 1-L_{\perp}\end{pmatrix}, \tag{8}$$

where the three independent real parameters $\gamma,\overline{P}_l,L_{\perp}$, which describe the shape of the inelastically excited target atom [1], are given by

$$\gamma=\frac{1}{2}\arg(\overline{P}_1+i\overline{P}_2), \tag{9}$$

$$\overline{P}_l=(\overline{P}_1^2+\overline{P}_2^2)^{1/2}, \tag{10}$$

$$L_{\perp}=-\overline{P}_3. \tag{11}$$

A. Pure polarization

If pure polarization is assumed, the measured P_i parameters can be directly related to the ideal reduced parameters via optical pumping parameters K_i:

$$P_i=K_i\overline{P}_i. \tag{12}$$

The coefficients K_i incorporate all aspects of the target state relevant to the collision dynamics. The target state σ is determined by the laser polarization, intensity, detuning, and linewidth, by the atomic beam density and divergence, and by the laser-atom interaction times. It can be calculated [4] or measured [6]. For pure polarization, the linear coefficients K_1 and K_2 are equal; they can be measured as the linear polarization of the fluorescence emitted in the scattering plane, at right angles to the laser polarization. K_3 is the circular polarization of fluorescence emitted in the direction of laser propagation [4,6].

B. Arbitrary polarization

It can be seen from Eqs. (5) that, for arbitrary polarization, there is no longer a direct relationship between each measured P_i and the corresponding ideal $\overline{P}_i$. Each P_i depends on *all* of the electron polarization sensitivities $\overline{P}_i$, each weighted by separate optical pumping coefficients which reflect the polarization-dependent target state. Using Eqs. (3)–(5), we find

$$P_1'=\frac{\kappa_{11}\overline{P}_1+\kappa_{12}\overline{P}_2}{1+\kappa_{13}\overline{P}_3}, \tag{13a}$$

$$P_2'=\frac{\kappa_{22}\overline{P}_2+\kappa_{21}\overline{P}_1}{1+\kappa_{23}\overline{P}_3}, \tag{13b}$$

$$P_3'=\frac{\kappa_{33}\overline{P}_3+\kappa_{32}\overline{P}_2}{1+\kappa_{31}\overline{P}_1}, \tag{13c}$$

where the prime indicates imperfect polarization. The coefficients κ again depend on the laser preparation of the excited state, that is, on the excited state density matrix terms, a–e, and hence on the laser polarization. $\kappa_{13,23}$ determine the effect of $\overline{P}_3$ influencing the $P_{1,2}$ measurements, and $\kappa_{31,32}$ determine the effect of $\overline{P}_{1,2}$ on the P_3 measurement. Note that these are quite different to the K_i coefficients used for the case of pure polarization.

For P_1 and P_2, we know that as the circular polarization contribution reduces to zero, the expressions for P_1' and P_2' devolve to the simple case of pure polarization; hence $\kappa_{12,13}$ and $\kappa_{21,23}$ must be small. Similarly, for P_3 measurements, we expect that $\kappa_{31,32}$ should be small. For small polarizations, we can then reduce these to lowest order in the polarization error:

$$P_1' = \kappa_{11}\overline{P}_1 + \kappa_{12}\overline{P}_2 - \kappa_{11}\kappa_{13}\overline{P}_1\overline{P}_3, \tag{14a}$$

$$P_2' = \kappa_{22}\overline{P}_2 + \kappa_{21}\overline{P}_1 - \kappa_{22}\kappa_{23}\overline{P}_2\overline{P}_3, \tag{14b}$$

$$P_3' = \kappa_{33}\overline{P}_3 + \kappa_{32}\overline{P}_2 - \kappa_{33}\kappa_{31}\overline{P}_1\overline{P}_3. \tag{14c}$$

For small polarization imperfections, we can expect the coefficients to be close to their values for perfect polarization, and so, for example, κ_{33} will be near unity while $\kappa_{31,32}$ will be small.

The effects of the unwanted polarization elements can be detected by studying the influence of the additional unwanted $\overline{P}$ components in a given P_i measurement. To appreciate this, we must first consider how polarization errors arise in practical apparatus.

IV. POLARIZER

The polarization errors depend on the design and implementation of the device used to polarize the laser beam and on additional elements in the beam path, such as mirrors and vacuum viewports. We consider a particular polarizer design to simplify the discussion, but the analysis can be applied straightforwardly to other systems. Potential systematic errors are identified for our polarizer, and then we consider the consequences of these errors to the target state preparation and therefore to measurements of the scattering density matrix.

Figure 2 shows our polarizer configuration, using a scheme apparently not previously used for superelastic experiments, but which offers significant advantages over other systems. This design, introduced briefly in [2], has since been used successfully by others [7].

Two rotatable quarter-wave retarders are used; each can be individually rotated, and using the different configurations listed, this arrangement provides linearly polarized light at any angle, or circularly polarized light of either helicity. All three polarization sensitivities P_i can be measured during a single experiment without changing optics. Conventional schemes using a single quarter-wave retarder with optional linear polarizer [8], or a polarizer with interchangeable waveplates [9], require reconfiguration of the polarizer in changing from $P_{1,2}$ to P_3, with possible difficulties in ensuring identical alignment of the laser beam, and of the polarization axis.

Errors in the polarization can arise from a rotational misalignment of the retarders ($\Delta\alpha$) or from deviations of the retardance ($\Delta\delta$). Additional errors due to birefringence of the vacuum viewport between polarizer and target atoms cause effects similar to retardance errors and hence are neglected here for simplicity. Note that other polarizing systems [8,9] produce systematic errors which can be reduced to equivalent misalignment or retardance errors.

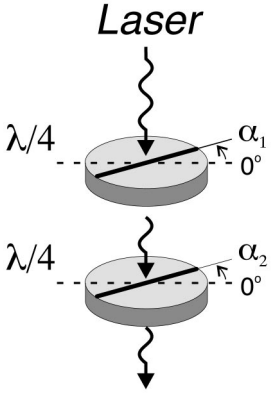

Polarization	α_1	α_2
RHC	0°	45°
LHC	0°	−45°
0°	45°	−45°
90°	45°	45°
45°	45°	0°
135°	45°	90°

FIG. 2. Polarizer for obtaining linearly polarized light at any angle, and circular polarization of either helicity, without removal or addition of optical elements. The laser is initially linearly polarized at 0°.

To evaluate the effects of these systematic errors, we described the laser polarization in terms of the usual Stokes polarization vector $\boldsymbol{S}$ [3]. The laser is initially linearly polarized at 0°, in our case using a Glan-Taylor prism with 10^5 extinction ratio, and so the input Stokes vector is

$$\boldsymbol{S}_{\rm in} \equiv \begin{pmatrix} S_0 \\ S_1 \\ S_2 \\ S_3 \end{pmatrix} = \begin{pmatrix} 1 \\ 1 \\ 0 \\ 0 \end{pmatrix}. \tag{15}$$

The polarization effects of the retarders are calculated using Mueller calculus, in which the retarders are defined by 4 $\times$4 matrices $\boldsymbol{R}$ [10]. For the polarizer in Fig. 2, we have

$$\boldsymbol{S}_{\rm out} = \boldsymbol{R}_2\boldsymbol{R}_1\boldsymbol{S}_{\rm in}, \tag{16}$$

where $\boldsymbol{R}_{1,2}$ define the two retarders, and $\boldsymbol{S}_{\rm out}$ is the final polarization state of the beam.

The general expression for a waveplate of retardation δ, with optic axis at angle α to the input linear polarization, is given by [11]

$$\boldsymbol{R}(\alpha,\delta)=\begin{pmatrix} 1 & 0 & 0 & 0 \\ 0 & \cos^2 2\alpha+\sin^2 2\alpha\cos\delta & \cos 2\alpha\sin 2\alpha(1-\cos\delta) & -\sin 2\alpha\sin\delta \\ 0 & \sin 2\alpha\cos 2\alpha(1-\cos\delta) & \sin^2 2\alpha+\cos^2 2\alpha\cos\delta & \cos 2\alpha\sin\delta \\ 0 & \sin 2\alpha\sin\delta & -\cos 2\alpha\sin\delta & \cos\delta \end{pmatrix}. \tag{17}$$

Including the errors for misalignment ($\Delta\alpha$) and retardance ($\Delta\delta$), the device matrices become

$$\boldsymbol{R}_i=\boldsymbol{R}(\alpha_i+\Delta\alpha_i,\pi/2+\Delta\delta_i) \tag{18}$$

for $i=1,2$. The final polarization can be calculated using Eq. (16) for each of the configurations shown in Fig. 2.

Taking all deviations $\Delta\alpha_{1,2}$ and $\Delta\delta_{1,2}$ to be small, we set $\boldsymbol{S}_{\rm out}=\boldsymbol{S}_{\rm out}^{\rm ideal}+\Delta\boldsymbol{S}_{\rm out}$, where $\Delta\boldsymbol{S}_{\rm out}$ is a (small) error, and to first order we find

$$\boldsymbol{S}_{0^\circ/90^\circ}\approx\begin{pmatrix}1\\ \pm 1\\ 0\\ 0\end{pmatrix}+\begin{pmatrix}0\\ 0\\ -2\Delta\alpha_1\pm 2\Delta\alpha_2\\ \pm\Delta\delta_1-\Delta\delta_2\end{pmatrix}, \tag{19a}$$

$$\boldsymbol{S}_{45^\circ/135^\circ}\approx\begin{pmatrix}1\\ 0\\ \pm 1\\ 0\end{pmatrix}+\begin{pmatrix}0\\ -\Delta\delta_1\mp 2\Delta\alpha_2\\ 0\\ \pm 2\Delta\alpha_1-\Delta\delta_2\end{pmatrix}, \tag{19b}$$

$$\boldsymbol{S}_{\rm RHC/LHC}\approx\begin{pmatrix}1\\ 0\\ 0\\ \pm 1\end{pmatrix}+\begin{pmatrix}0\\ \mp 2\Delta\alpha_1-\Delta\delta_2\\ 2\Delta\alpha_1-2\Delta\alpha_2\\ 0\end{pmatrix}. \tag{19c}$$

It can be seen that the different systematic errors $\Delta\alpha_{1,2}$ and $\Delta\delta_{1,2}$ combine linearly, and so we can consider these problems in terms of any one error alone, for example, $\Delta\alpha_1$:

$$\boldsymbol{S}_{0^\circ/90^\circ}\approx\begin{pmatrix}1\\ \pm 1\\ -2\Delta\alpha_1\\ 0\end{pmatrix}, \tag{20a}$$

$$\boldsymbol{S}_{45^\circ/135^\circ}\approx\begin{pmatrix}1\\ 0\\ \pm 1\\ \pm 2\Delta\alpha_1\end{pmatrix}, \tag{20b}$$

$$\boldsymbol{S}_{\rm RHC/LHC}\approx\begin{pmatrix}1\\ \mp 2\Delta\alpha_1\\ 2\Delta\alpha_1\\ \pm 1\end{pmatrix}. \tag{20c}$$

V. IMPERFECT POLARIZATION

From Sec. II, we have the scattering rate for elliptically polarized light; from Sec. III the polarization sensitivities P_i for imperfect polarizations; and from Sec. IV the kinds of polarization impurities that can be expected for a real apparatus. Using these arguments, we can see how experimental imperfections lead to systematic errors in the measured polarization sensitivities and hence in the collisional density matrix.

It can be seen from Eq. (20a) that for P_1 measurements, which rely on measuring the scattering rate with $\boldsymbol{S}_{0^\circ}$ and $\boldsymbol{S}_{90^\circ}$ polarizations, there is a small contribution of $-2\Delta\alpha_1$ to the S_2 component for both polarization angles. This has the effect of a small fixed component of laser light at $\phi=45^\circ$, in addition to the majority component polarized at $\phi=0^\circ$ or 90°. Since P_1 depends on the difference in scattering rates for these two laser polarizations, the small component cancels. Of course, this is a simplification, since the $\phi=45^\circ$ polarization error will in general have different effects on the target state when it is optically pumped at $\phi=0^\circ$ and $\phi=90^\circ$, but such differences are second-order effects.

For P_2 measurements, there is again a $2\Delta\alpha_1$ component, this time in the S_3 circular component of the Stokes vectors [Eq. (20b)]. In this case, however, the sign of the error changes with the polarization angle $\phi=45^\circ,135^\circ$. Thus in measuring the scattering rate $\mathcal{I}_{45}$ there is a RHC component, and in measuring $\mathcal{I}_{135}$ there is a LHC component; the P_2 measurement therefore includes a significant contribution from $\overline{P}_3$.

Recalling Eq. (14b),

$$P_2'=\kappa_{22}\overline{P}_2+\kappa_{21}\overline{P}_1-\kappa_{22}\kappa_{23}\overline{P}_2\overline{P}_3\approx\kappa_{22}\overline{P}_2+\kappa_{22}\kappa_{23}\overline{P}_2\overline{P}_3 \equiv P_2+\Delta P_2, \tag{21}$$

where P_2 is the expected value for pure polarization, P_2' is the measured value with imperfect polarization, and ΔP_2 is the error. The pumping parameter κ_{23} depends on the circular component of the polarization. For perfectly linear light, $\kappa_{23}=0$, and scales approximately linearly for small circular component. The circular polarization is given by $2\Delta\alpha_1$, and we write

$$\Delta P_2=\varepsilon_{23}(2\Delta\alpha_1)\overline{P}_2\overline{P}_3, \tag{22}$$

where ε_{23} is a proportionality constant which gives the effect on P_2 due to the circular polarization and P_3 components.

Similarly, measurements of P_3 will include contributions from P_1 due to the alternating sign of the error in the Stokes S_1 component.

TABLE I. Scattering angles and polarization sensitivities used to investigate contributions from imperfect laser polarization. Reduced polarization sensitivities can be calculated using Eq. (12) where $K_1=K_2=0.575$ and $K_3=1.00$ [2].

Energy	θ_e	P_1	P_2	P_3
5.2/7.0 eV	35°	−0.069	−0.10	−0.90
12/13.8 eV	75°	0.47	0.05	−0.55
12/13.8 eV	135°	0.37	−0.35	0.44

VI. EXPERIMENT

The effects of imperfect polarization have been established experimentally, by measuring the polarization sensitivities P_i while varying the ellipticity of the laser polarization, at angles and energies chosen to illustrate the effects as shown in Table I.

The data were taken in a series of the superelastic scattering experiments on the $2\,^2P$ state of Li^6 [2]. The representation 5.2/7.0 eV means that the incident energy was 5.2 eV and electrons of energy 7.0 eV were detected.

Figure 3 shows the measured values of P_i for $E_0=7.0$ eV and $\theta_e=35°$, for various misalignments $\Delta\alpha_1$ of the first waveplate in the polarizer.

The results for P_2, in particular, demonstrate the effects, with a strong contribution from $\overline{P_3}$. The dependence is approximately linear, and using Eq. (22) with the tabulated values for $\overline{P_{2,3}}$ we find $\varepsilon_{23}=\Delta P_2/(2\Delta\alpha_1\overline{P_2}\overline{P_3})=12.7$. The slope can also be calculated numerically from Eq. (21) and using optical pumping calculations to find κ_{23} for various $\Delta\alpha$.

As expected, the depolarization effects on P_1 are small, since the polarization error does not change sign with $\phi=0°,90°$. There is also only negligible variation in P_3 with $\Delta\alpha_1$, as expected for the small value of P_1. However, additional measurements at $\theta_e=75°$ and 135°, where P_1 is much larger, also show small effects, with a negligible value for $P_3/\Delta\alpha_1$. Clearly the optical pumping factor κ_{31} of Eq. (14c), which weights the contribution of $\overline{P_1}$ to P_3, is small.

The errors in $\overline{P_{1,2}}$ are proportional to $\overline{P_3}$ and therefore depend on the scattering angle. Figure 4 shows the *expected* errors in P_2 over a broad range of scattering angles, at an

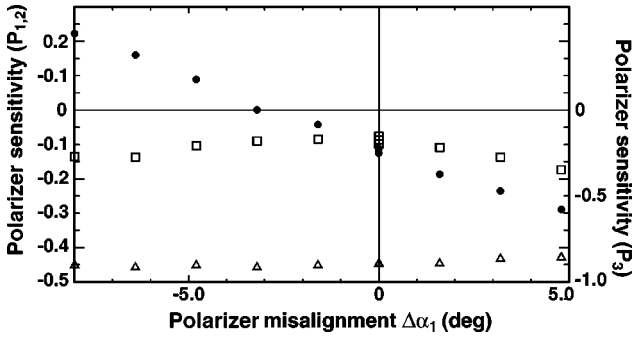

FIG. 3. Measured polarization sensitivities P_i for energy 5.2/7.0 eV and scattering angle $\theta_e=35°$, as a function of the polarization error introduced by misalignment of the first retarder, $\Delta\alpha_1$. □ $=P_1$, ● $=P_2$, △ $=P_3$.

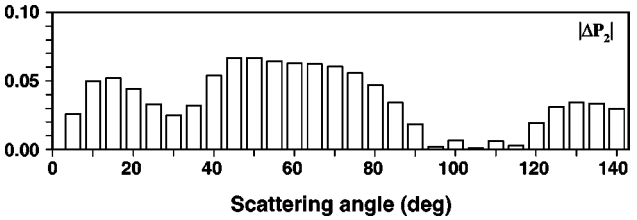

FIG. 4. Systematic uncertainty in P_2 caused by a small circular polarization component, as a function of scattering angle θ_e, for electron scattering by Li^6 at an energy of 5.2/7.0 eV.

energy of 5.2/7.0 eV. These are calculated based on the measurements of ε_{23} made at 35° and given the measurements of P_2 and P_3 at the scattering angles shown.

VII. ESTIMATION OF SYSTEMATIC ERRORS

An estimate of the errors caused by imperfect polarization can be made without such detailed analysis, simply by comparing the measured results for P_1 at positive and negative scattering angles. The polarization sensitivities $P_1(\theta_e)$ and $P_3(\theta_e)$ have different parities: P_3 changes sign with θ_e whereas P_1 does not. Hence, in a form similar to Eq. (21),

$$P_1'(+\theta_e)=P_1(\theta_e)-|\Delta P_1|\equiv P_1(\theta_e)+\eta_{13}|\overline{P_3}|, \quad (23)$$

where η_{13} reflects the contribution of $\overline{P_3}$ due to unspecified polarization errors, and

$$P_1'(-\theta_e)=P_1(\theta_e)-\eta_{13}|\overline{P_3}| \quad (24)$$

so that

$$\eta_{13}=\frac{1}{2}\,\frac{P_1'(+\theta_e)-P_1'(-\theta_e)}{\overline{P_3}(\theta_e)}. \quad (25)$$

Hence by measuring P_1 at $\pm\theta_e$, for some angle where $\overline{P_3}$ is large, η_{13} gives an estimate of the undesired circular component in the laser polarization, and hence of the retarder misalignment $\Delta\alpha$ when polarization angles $\phi=0°,90°$ are desired.

Similar measurements can be made for $\phi=45°,135°$. Again, P_1 must be measured, but in this case the electron source and detector are both rotated by 45°. The polarizer is then still set for 45°,135° with respect to the original scattering reference frame, but at 0°,90° with respect to the new positions of the electron source and detector.

It is important to emphasize that simply averaging the P_1 measurements for $\pm\theta_e$ removes the final errors to first order. Alternately, while taking measurements of P_1 at $\pm\theta_e$, the polarizer can be adjusted to obtain symmetry and therefore minimize polarization errors.

Similar arguments can be used to investigate the influence of linear errors, that is, misalignment of the polarization ellipse, adjusting the second retarder to induce the appropriate effects.

VIII. SUMMARY

We have investigated the systematic causes and effects of imperfect laser polarization in superelastic scattering experiments. We have derived an expression for the superelastic scattering rate from target atoms optically pumped with elliptically polarized light, and used this to show how secondary polarization components cause contributions from all components of the scattering density matrix. In particular, we find that in measuring the scattering for linearly polarized light, the errors are proportional to $\overline{P}_3$, the scattering sensitivity to circular light, and to the undesired circular polarization component. The polarization impurity can be determined during the collision experiment by investigating scattering from positive and negative angles, and used to correct the polarizing device or the scattering measurements. Finally, we have described in detail a new polarizer design which generates both linear and circular polarizations, allowing measurement of all scattering polarization sensitivities without requiring interchange of optical elements.

[1] N. Andersen, J. W. Gallagher, and I. V. Hertel, Phys. Rep. **165**, 1 (1988).
[2] V. Karaganov, I. Bray, P. J. O. Teubner, and P. M. Farrell, Phys. Rev. A **54**, R9 (1996); V. Karaganov, I. Bray, and P. J. O. Teubner, J. Phys. B **26**, L187 (1998).
[3] M. Born and E. Wolf, *Principles of Optics*, 6th ed. (Pergamon Press, Oxford, 1980).
[4] P. M. Farrell, W. R. MacGillivray, and M. C. Standage, Phys. Rev. A **44**, 1828 (1991).
[5] B. T. H. Varcoe, R. T. Sang, W. R. MacGillivray, M. C. Standage, and P. M. Farrell, J. Mod. Opt. **46**, 787 (1999).
[6] A. Fischer and I. V. Hertel, Z. Phys. A **304**, 103 (1982).
[7] M. Shurgalin, A. J. Murray, W. R. MacGillivray, and M. C. Standage, J. Phys. B **31**, 4205 (1998).
[8] R. E. Scholten, G. F. Shen, and P. J. O. Teubner, J. Phys. B **26**, 987 (1993).
[9] Y. Li and P. W. Zetner, Phys. Rev. A **49**, 950 (1994).
[10] W. A. Shurcliff, *Polarised Light: Production and Use* (Harvard University Press, Cambridge, MA, 1996).
[11] M. J. Walker, Am. J. Phys. **22**, 170 (1954).
[12] K. Blum, *Density Matrix Theory and Applications*, 2nd ed. (Plenum Press, New York, 1996).